Evapotranspiration dynamics and their drivers in a temperate mixed forest in northeast China

Xiaoying Wang[1], Xianjin Zhu[1,2], Mingjie Xu[1,2], RiHong Wen[1], Qingyu Jia[1], YanBing Xie[1] and Hongda Ma[3]

[1] Institute of Atmospheric Environment, China Meteorological Administration, Shenyang, People's Republic of China
[2] Shenyang Agricultural University, College of Agronomy, Shenyang, People's Republic of China
[3] Yichun Wuying District Meteorological Service, Yichun, People's Republic of China

Corresponding authors
Xianjin Zhu, xianjin@syau.edu.cn
RiHong Wen,
wenrihong1016@163.com

ABSTRACT

Evapotranspiration (ET) is a vital part of the global water cycle and is closely related to carbon sequestration. Analysing ET dynamics and their drivers would benefit for improving our understanding of the global water and carbon cycles. Using an eddy covariance (EC) approach, we analysed ET dynamics and their drivers in a temperate mixed forest over northeast China from 2016 to 2017. The results showed that 43.55% of our eddy covariance data passed the quality control. In addition, the energy balance ratio was 0.62, indicating that measurements were reliable. The measured ET showed clear single peak patterns with seasonal and diurnal variations. The daily ET ranged from 0 to 7.75 mm d^{-1} and the hourly ET ranged from 0 to 0.28 mm h^{-1}. The ranges of hourly ET floated from 0 to 0.05 mm h^{-1} at non-growing season (November to April) while ranged from 0 to 0.28 mm h^{-1} at active growing season (May to October). The diurnal ET dynamics during the non-growing season were driven by air temperature (T_a), but were governed by global radiation (R_g) during the active growing season. Leaf area index (LAI) comprehensively reflected the variations of T_a and R_g, and was found to be the primary factor shaping the seasonal dynamics of ET. The annual ET rates were 501.91 ± 5.30 mm year^{-1} and 554.60 ± 11.24 mm year^{-1} for 2016 and 2017, respectively. Therefore, energy supply, represented by T_a and R_g, governed ET dynamics in our temperate mixed forest, while variables representing the energy supply affecting ET dynamics differed among seasons and time scales. ET dynamics indicated that a temperate mixed forest is important to the global water cycle. Our results improved our understanding of ET dynamics in the studied region.

INTRODUCTION

Evapotranspiration (ET) is defined as the water lost as vapour rising from the land to the atmosphere. It is a vital part of the global water cycle (*Kool et al., 2014*; *Wang et al.,*

2010; *Wang & Dickinson, 2012*). ET is also closely associated with carbon sequestration as water loss and carbon sequestration both primarily appear in the stoma of a plant (*Chapin, Matson & Mooney, 2012*), which made ET closely associate with the global carbon cycle (*Zhu et al., 2015b*). Analysing the dynamics of ET and their drivers is beneficial for understanding the mechanisms underlying ET dynamics, thus accurately modeling ET. This also results in a better understanding of the global water and carbon cycles (*Anapalli et al., 2020*).

Analysing ET dynamics and their drivers requires accurate measurements (*Li et al., 2009*; *Rana & Katerji, 2000*; *Wang & Dickinson, 2012*). The micrometeorological theory known as eddy covariance (EC) has been widely used in measuring ET for its *in-situ*, continuous, and accurate measurements (*Baldocchi & Ryu, 2011*; *Drexler et al., 2004*; *Tanaka et al., 2008*). Many studies have analysed ET dynamics and their drivers for various ecosystems using EC (*Cristiano et al., 2015*; *Kume et al., 2011*; *Ma et al., 2015*; *Song et al., 2017*; *Xu et al., 2014*; *Yue et al., 2019*). Results showed that daily accumulated ET and their annual values differed among ecosystems (*Kumagai et al., 2005*; *Li et al., 2010*; *Tong et al., 2017*). Some studies have analysed ET dynamics and their drivers for temperate forests in North America (*Schaefer et al., 2014*; *Wang et al., 2015*; *Wehr et al., 2017*), Europe (*Gielen et al., 2010*; *Pita et al., 2013*; *Soubie et al., 2016*), and Asia (*Tsuruta et al., 2016*; *Wu et al., 2013*; *Zhang et al., 2012*). Carbon fluxes (*Ohtsuka et al., 2005*; *Saigusa et al., 2002*) and resource use efficiency (*Okada, Takagi & Nishida, 2019*) in temperate mixed forests over Asia have also been intensively reported, while less attention has been given to ET dynamics and what drives them in these ecosystems, which made the ET dynamics in this region poorly understood. In addition, temperate mixed forests over Asia are climax communities and the succession climax indicates the potential of this region to regulate regional energy and mass cycles (*Zhang, Han & Yu, 2006*; *Zhang et al., 2006b*). Analysing ET dynamics and their drivers in temperate mixed forests will improve our understanding of ET dynamics in this region, which benefited for revealing the potential role of this region in global water cycles.

We analysed ET dynamics and their drivers for a temperate mixed forest based on EC measurements in a broad-leaved Korean pine forest in northeast China. The main objectives of this study were: (1) to reveal ET dynamics for a temperate mixed forest in Northeast China, (2) to clarify the major drivers of ET dynamics, and (3) to reveal the magnitude of annual ET in this unique ecosystem. In order to address these objectives, we first addressed the energy balance closure of the eddy covariance measurements, which was directly related to the ET measurements (*Wilson et al., 2002*). We then showed the dynamics of ET and their environmental factors, including solar radiation (R_g), air temperature (T_a), relative humidity (RH), precipitation, and leaf area index (LAI) to determine the drivers of ET dynamics. Then the drivers of ET dynamics were performed. Our results elucidate the understanding of ET dynamics and ET modeling over a temperate mixed forest, which improves our understanding of the water cycle processes and their linked carbon cycles.

MATERIALS AND METHODS

Site description

EC measurements were taken at the Yichun broad-leaved Korean pine forest experimental station (48.2292°N, 129.2661°E, 342 m.a.s.l) from January 2016 to December 2017. This station was located in the middle of Heilongjiang Province, which was the northeastern-most province of China (Fig. 1A). The experimental ecosystem had a flat topography with an evenly distributed mixed forest (14,141 hm^{-2}). The mean fetch of the tower in all directions was lower than 400 m, with the prevailing southwest and northeast wind directions (Fig. 1B). The forest was primarily comprised of Korean Pine (*Pinus koraiensis*), Mongolian Oak (*Quercus mongolica)*, Amur Linden (*Tilia amurensis*), and Maple Birch (*Betula costata*), with a density of 1,152 plants per hm^{-2} and an average stand age of 220-years (Fig. 1C). Korean Pine (*Pinus koraiensis*), Mongolian Oak (*Quercus mongolica)*, Amur Linden (*Tilia amurensis*), and Maple Birch (*Betula costata*) accounted for 10–15% of all plants in the study area, respectively. The mean canopy height was 26 m with a maximum and minimum LAI of 6.2 and 0.5 m^2 m^{-2}, respectively. The experimental forest had a temperate continental climate with a long-term mean annual air temperature (MAT) of 0.63 °C and a mean annual precipitation (MAP) of 610.7 mm. The highest T_a appeared in July with a long-term mean (1981–2010) value of 20.4 °C, while the lowest T_a occurred in January with a value of −22.5 °C. The greatest amount of precipitation occurred in July (147 mm), while the lowest precipitation occurred in February (6.7 mm). Precipitation was commonly seen as snowfall from November to April, and totaled approximately 90 mm $year^{-1}$. The soil in the experimental ecosystem was characterized as dark brown soil with high soil organic matter content.

Data measurements

We employed a flux tower with a height of 70 m to measure the ET and conventional meteorological variable dynamics.

The EC system was composed of a datalogger (Model CR5000; Campbell Scientific Inc., Logan, UT, USA), a 3-D sonic anemometer (Model CSAT3; Campbell Scientific Inc., Logan, UT, USA), and an infrared gas analyzer (Model LI-7500; Licor Inc., Lincoln, NE, USA). These were used to measure the net H_2O exchange between the terrestrial ecosystem and the atmosphere, which can be considered as the ET. The EC sensors, including CSAT3 and LI-7500, were mounted at a height of 50 m, which was about twice of the canopy height. The EC measurement sampled the raw data with a frequency of 20 Hz and recorded the flux data at 30-min intervals.

Conventional meteorological variables were also measured, including air temperature (T_a), relative humidity (RH), soil temperature (T_s), precipitation, and soil heat flux (G). T_a and RH were measured at different heights (1.5, 20, 30, 40, 50, 60 m) with shielded and aspirated probes (Model HMP45C; Campbell Scientific Inc., Logan, UT, USA). T_s was measured using thermocouple probes (Model 105T; Campbell Scientific Inc., Logan, UT, USA) at different depths (0, 5, 10, 15, 20, 40, 80, 160, 320 cm). Precipitation was recorded with a rain gauge (Model 52203; R.M. Young Company, Traverse City, MI, USA)
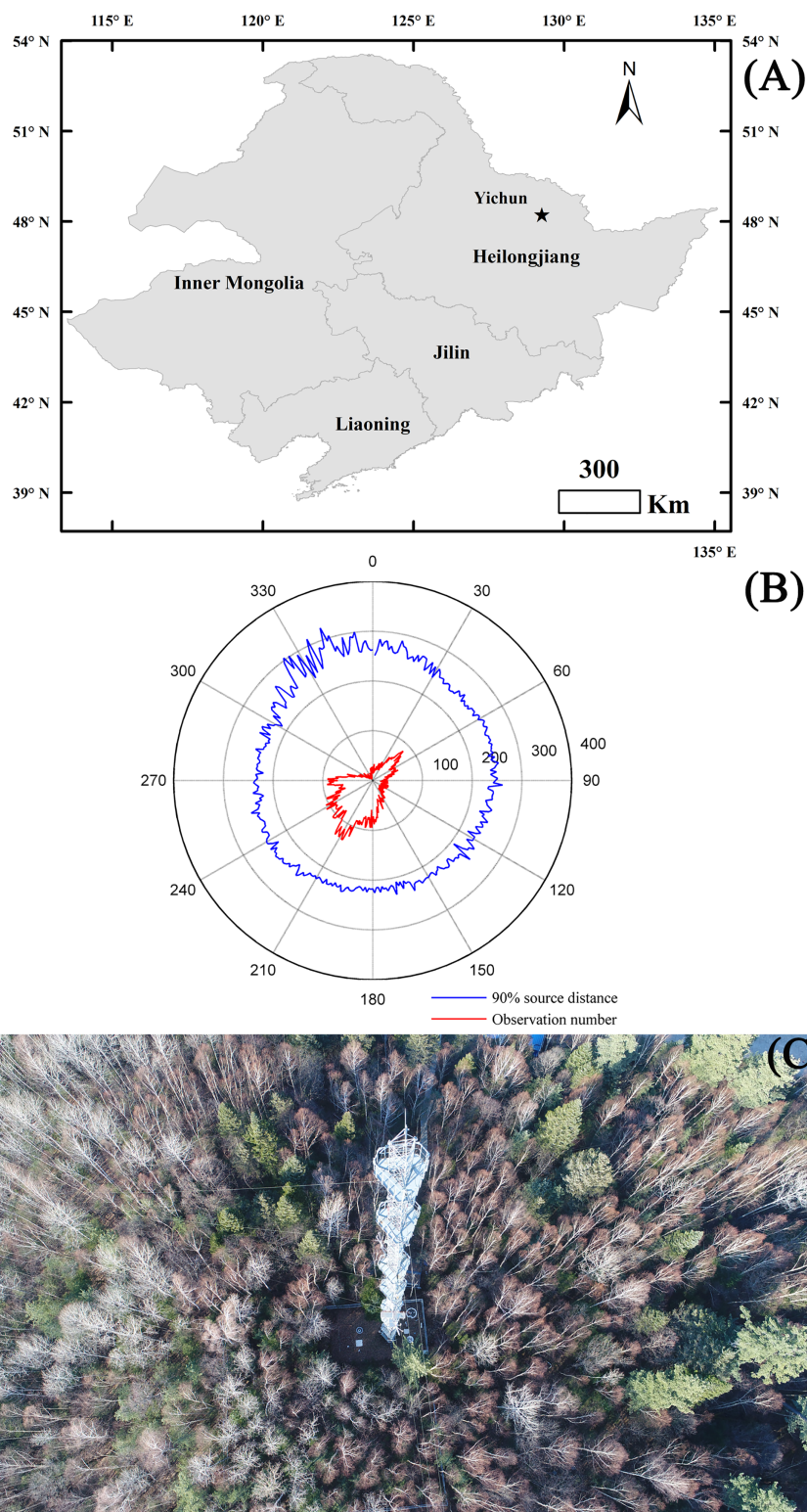
Figure 1 Site information. The ecosystem location (A) and its main characteristics, including the main wind directions and footprint (B), and the main plant composition (C). The footprint was calculated following *Kljun et al. (2004)* after calculating the mean of each degree. The maps of panel (A) were made by ArcGIS 10.0 (http://www.esri.com/software/arcgis).

at the height of 38 m. G was measured with two flux plates (Model HFP01SC; Campbell Scientific Inc., Logan, UT, USA) at depths of 5 and 15 cm, respectively. Conventional meteorological variables were measured at a frequency of 1 s and recorded at 30-min intervals with dataloggers (Model CR10X & CR23X; Campbell Scientific Inc., Logan, UT, USA).

Radiation data, including global radiation (R_g), reflected radiation (R_r), downward long wave radiation (DLR), and upward long wave radiation (ULR), were measured with a radiation heat balance station (CAMS620-SP, Huatron, China) at 1-h intervals. The measured 1-h data were linearly interpolated into half-hour scale to match the time series of ET and other environmental variables. Net radiation (R_n) was calculated as the sum of net short-wave radiation (R_{ns}) and net long-wave radiation (R_{nl}), where R_{ns} was the difference between R_g and R_r while R_{nl} was the difference between DLR and ULR.

Data processing

Flux data processing

The net H_2O exchange, which was deemed as ET and latent heat (LE), was calculated as the covariance between vertical wind speed (v) fluctuations and water vapor concentration fluctuations. The spikes of wind speeds and H_2O concentrations were detected and deleted based on CSAT3 measuring three-dimension wind speeds and LI-7500 measuring H_2O concentrations (*Vickers & Mahrt, 1997*). The raw ET was deemed as missing if the missing or deleted data were more than 3,600 in each half-hour (10% of all measurements) (*Wen et al., 2010*). The raw ET was calculated as the covariance of vertical wind (v) speed fluctuations and H_2O concentration fluctuations using the despiked data. The calculated raw fluxes were derived from a three-dimensional rotation (*Aubinet et al., 2000*), Webb, Pearman and Leuning (WPL) correction (*Webb, Pearman & Leuning, 1980*), spectral correction for high-frequency losses (*Moncrieff et al., 1997*), low-frequency losses (*Moncrieff et al., 2005*), physical instrument separation losses (*Horst & Lenschow, 2009*), storage calculation (*Hollinger et al., 1994*), and footprint analysis (*Kljun et al., 2004*) calculated using online Eddypro 4.2 software (Licor Inc., Lincoln, NE, USA). The Eddypro proceeding water vapor fluxes were flagged with different numbers, where 0 and 1 indicated high quality fluxes that were suitable for ET dynamics analysis, while 2 indicated poor quality fluxes that should be discarded. The Eddypro data for ET flagged as 0 and 1 were further filtered for precipitation, threshold deleting, and low turbulence. The ET fluxes selected during a precipitation event and the following half hour were deleted as the sensors may suffer from moisture contact. The selected ET lower than −0.32 mm h^{-1} or higher than 1.30 mm per hour were deleted. Low turbulence was determined by the u* threshold, which was calculated following *Reichstein et al. (2005)* using u*, CO_2 fluxes, and T_a. The calculated u* thresholds were 0.25 and 0.21 m s^{-1} for 2016 and 2017, respectively. The data coverage after data quality control was 42.55% and 44.55% for 2016 and 2017, respectively. However, the data coverage showed obvious differences between daytime and nighttime. During the daytime, the data coverage was 66.66% and 66.28% for 2016 and 2017, respectively. However, nighttime only had 18.48% and 22.82% data coverage for 2016 and 2017, respectively. This was primarily affected by the low turbulence at night.

The ET data gaps were filled using the look-up table method (*Falge et al., 2001a*; *Reichstein et al., 2005*) based on T_a, vapor pressure deficit (VPD), and R_n.

CO_2 fluxes were measured simultaneously using the same EC system and were calculated as the covariance between vertical wind speed (v) fluctuations and CO_2 concentration fluctuations. Heat fluxes (H) were calculated as the covariance between vertical wind speed (v) fluctuations and air temperature fluctuations. The raw H fluxes suffered from quality control issues similar to those of ET.

G was also subjected to quality control by threshold values. Data gaps for G were linearly interpolated for gaps of less than 2 h but were filled using the mean diurnal variation (MDV) method for longer periods (*Falge et al., 2001b*).

Auxiliary data processing

The auxiliary data including conventional meteorological data and biotic data were also subjected to data quality controls and gap-fillings.

T_a and RH above the canopy (at the height of 30 m) were used to analyze the drivers of ET dynamics. The qualities of T_a and RH were firstly controlled through threshold values. The measured T_a lower than -50 °C or higher than 50 °C were deleted, while the threshold values of RH were 0% and 100%. In addition, the measured T_a and RH lower than 70% or higher than 130% of the mean corresponding values of other layers were deleted. The data gaps of meteorological variables (including T_a and RH) were filled using the linear interpolation for gaps of less than 2 h. The remaining data gaps were firstly filled with the corresponding variables in neighboring layers. Then the remaining data gaps were filled with the mean diurnal variation (MDV) method (*Falge et al., 2001b*). VPD was then calculated as the difference between the actual and saturation vapor pressures based on the measured RH and T_a.

Precipitation data were quality checked and any gaps were filled using manual observations from a meteorological station affiliated with the Chinese Bureau of Meteorology, which was located approximately 18 km away from the observation tower.

R_g was quality controlled with spikes deletion. R_g data lower than 0 or higher than 1,300 W m^{-2} were removed. The data gaps of R_g were filled using the linear interpolation for gaps of less than 2 h, while the remaining data gaps were filled with the MDV method (*Falge et al., 2001b*).

R_n was also quality checked with spikes deletion used to estimate the energy balance closure. First, short wave radiation data lower than 0 or higher than 1,300 W m^{-2} were removed. Second, long wave radiation data lower than 100 W m^{-2} or higher than 600 W m^{-2} were removed. Only data passing the quality control were used to calculate R_n.

LAI was downloaded from the Moderate Resolution Imaging Spectroradiometer (MODIS) database with a spatial resolution of 500 m and a temporal variation of 4 days (https://modis.ornl.gov/subsetdata). In addition, the pixels from the surrounding 1 km area were also downloaded to avoid potential noises in a single pixel, which all had the same mixed forest. The downloaded LAI were linearly interpolated into a daily scale.

Data analysis

Energy balance closure assessment

We quantified the energy balance closure using two methods to validate the performance of the eddy covariance measurements. The first method derived the linear regression between the half-hour dependent flux variables *(LE + H)* and the available energy $(R_n - G)$ from the ordinary least squares (OLSs) relationship (*Li et al., 2005*). The regression coefficients, including the slope and the intercept, were used to evaluate the performance of energy balance closure. The ideal closure was reflected by a one slope and a zero intercept. The second method derived the cumulative sum of *LE + H* and available energy $(R_n - G)$ over measuring period and calculated the energy balance ratio (EBR) as follows:

$$EBR = \mathrm{sum}(LE + H)/\mathrm{sum}(R_n - G) \tag{1}$$

Only data directly measured and passing the quality control were used to calculate the energy balance closure. All available data were first potted to generate the energy balance closure during the measuring period. Then the whole year was divided into the active growing season (May-October) and the non-growing season (November to April), to generate the energy balance closure at different seasons.

ET dynamics and their drivers

Daily ET and environmental variables of each year were described to illustrate their seasonal dynamics. These were then used to reveal the drivers of the seasonal dynamics of ET. Only the data measured above the canopy (30 m) was used, although multilayer observations of T_a, RH, and VPD were obtained. To avoid the confusion of gap-filling data in representing ET seasonal dynamics and their drivers, we only used daily data during days having more than 20 (including 20) directly measured and passing the quality control data. Setting 20 as the minimum data number sourced from the following four aspects. First, the missing of ET primarily resulting from low turbulence during nighttime made no day have all half-hour data directly measured. Second, data gaps were primarily caused by ET missing as nearly all R_g were directly measured when the number of directly measured ET were over 20. Third, the small ET values during nighttime made the uncertainties in gap-filling contribute little to the daily accumulated values. Fourth, the occasionally appearing data gaps during daytime could be linear interpolated with high confidence.

The data from an entire year were divided into two groups: active growing season and non-growing season. The active growing season lasted from May to October and the non-growing season included the remaining months. We calculated the mean ET for each group over each half-hour and their corresponding variables, including T_a, R_g, and VPD, to represent the diurnal variations in different seasons. Only data directly measured and passing the quality control were used. Each available half-hour data point in each group was used to analyse the drivers of the diurnal variations of ET. Each year data were used seperately to validate the results from each year.

Though R_n was the direct variable reflecting the available energy, the calculation of R_n may be inaccurate as the bad sensors especially the long wave radiation sensors. Therefore, R_g was used to replace R_n to reveal the drivers of ET dynamics.

Uncertainty analysis

A simple Monte Carlo experiment was conducted to assess the uncertainty in the annual estimates of ET following *Desai et al. (2005)*. A random number generator was used to remove 10–50% of the existing observed data. The generated data gaps were then randomly selected and filled with modeled ET (described in Flux processing), which was run 100 times for each year (2016 and 2017).

Statistical analysis

MATLAB 2014a (Mathworks Inc., Natick, MA, USA) was used to process the data including the flux quality control and gap filling. Linear regression and non-linear regression were used to analyse the effects of various factors on dynamics (including the diurnal and seasonal dynamics) of ET. Stepwise regression was used to analyze the multiple linear regression on ET seasonal variations. The minimum P-value for a variable to be added or removed from the model in the stepwise regression was 0.10. A path-analysis was conducted to evaluate the dependence of ET on various factors. The significant level was set to $\alpha = 0.05$.

RESULTS

The energy balance closure

The energy balance closure indicated by the regression slope between the available energy ($R_n - G$) and energy fluxes ($LE + H$) (Fig. 2), suggested that our ecosystem experienced an energy imbalance. The slope between $R_n - G$ and $LE + H$ during the measuring period was 0.54, with an intercept of 13.87 W m^{-2} (Fig. 2A), which was obviously lower than 1. Additionally, different seasons had divergent regression slopes (Figs. 2B and 2C). During the active growing season, the regression slope could be 0.56 with an intercept of 21.68 W m^{-2} (Fig. 2B). Though the regression slope during active growing season was less than 1, it was still higher than that of the whole period (Fig. 3A) and the non-growing season, specifically (Fig. 2C). The regression slope during the non-growing season was only 0.39, with an intercept of 8.88 W m^{-2} (Fig. 2C).

The energy balance closure, as indicated by the energy balance ratio (EBR), also reflected the energy imbalance of the studied ecosystem. During the measuring period, EBR was 0.62 (Fig. 2A), which was also clearly lower than 1. However, the EBR differed among seasons (Figs. 2B and 2C). During the active growing season, the EBR measured 0.66 (Fig. 2B), which was still lower than 1 but higher than that of the whole period (Fig. 2A) and the non-growing season (Fig. 2C). The EBR during the non-growing season only measured 0.47 (Fig. 2C).

The seasonal dynamics of ET and environmental factors

ET and its related environmental factors all exhibited obvious seasonal dynamics (Fig. 3).

Environmental factors including T_a, VPD, R_g, precipitation, and LAI all exhibited obvious single peak seasonal dynamics (Figs. 3A–3F). T_a ranged from −17 to 29 °C, with the highest values appearing at July, which was consistent across both years measured (Fig. 3A). VPD had higher values during the active growing season and lower values during
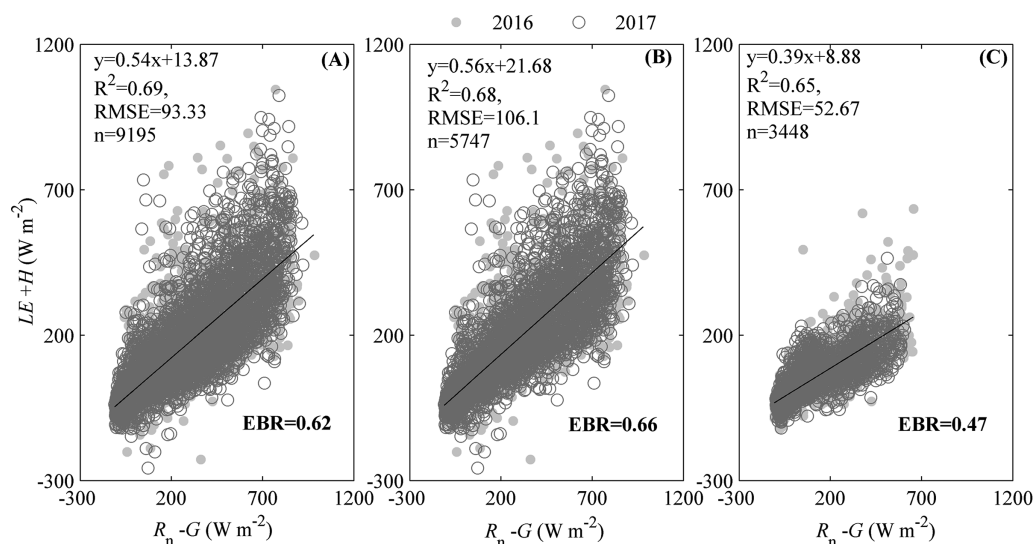
Figure 2 **The energy balance closure calculated by the ordinary least squares (OLSs) relationship and energy balance ratio (EBR).** The OLSs relationship was calculated between the available energy (R_n–G) and the energy fluxes in the studied ecosystem during measuring period. The available energy was the difference between the net radiation (R_n) and soil heat flux (G). The energy fluxes were the sum of heat fluxes (H) and latent heat fluxes (LE). EBR was calculated as the ratio of total energy fluxes to available energy during the measuring period, was also calculated. Only data passing quality control were used. The energy balance closure was calculated during the whole measuring period (A), the active growing season (B), and non-growing season (C).

the non-growing season; the highest VPD appeared in May (Fig. 3C). R_g ranged from 0.2 to 25 MJ m^{-2} d^{-1} and had similar dynamics to those of VPD (Fig. 3D). Precipitation also differed among seasons, with the most precipitation occurring from May to September (Fig. 3E). LAI ranged from 0.2 to 4.9 m^2 m^{-2}, with the highest values in July. RH did not show much variation across the months (Fig. 3B).

The seasonal dynamics of ET also exhibited a single-peak pattern, with the higher values appearing in the summer (Fig. 3F). However, the peak values of the seasonal dynamics of ET differed between the years measured (Fig. 3F). In 2016, ET achieved its peak (>6 mm d^{-1}) in the middle of July and then decreased. In 2017, ET showed an increasing trend until the end of August, and achieved its highest value for 2017 (>7 mm d^{-1}) at the end of August.

The diurnal dynamics of ET and environmental factors

ET and environmental factors all exhibited similar, obvious diurnal dynamics during the active growing season and non-growing season, but their values differed between seasons (Fig. 4).

During the day, T_a and R_g both showed single-peak patterns (Figs. 4A, 4B and 4G, 4H). These factors did not vary much from midnight to sunrise, but rapidly increased after sunrise, achieved their peak values around noon, and started to decrease at sunset. The factors were then stable until the end of the day. The time that T_a achieved its peak values (approximately 13:00 local time) was later than that of R_g. However, RH exhibited a concave shape (Figs. 4C and 4D), which indicated that RH began to decrease
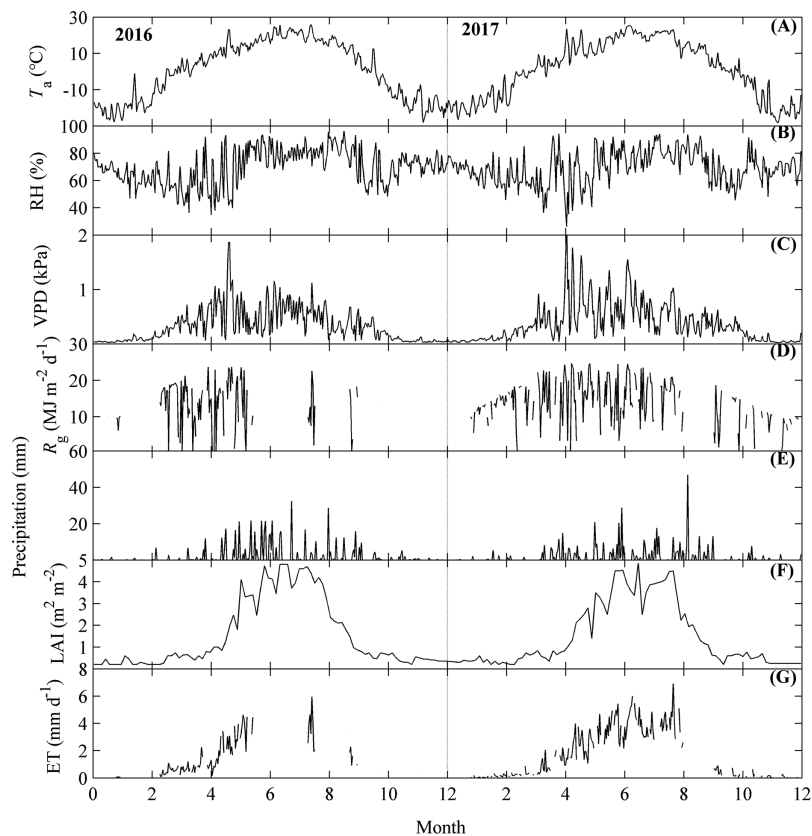
Figure 3 The seasonal dynamics of environmental factors and evapotranspiration (ET).
Environmental factors included air temperature (T_a, A), relative humidity (RH, B), vapor pressure deficit (VPD, C), global radiation (R_g, D), precipitation (E), and leaf area index (LAI, F). Seasonal variations of T_a, RH, VPD, and LAI were calculated as their daily mean values, while those of R_g, precipitation and ET (G) were calculated by their daily accumulated values. Only daily data during days having more than 20 (including 20) directly measured and passing the quality control data were used.

after sunrise. VPD did not vary much during the non-growing season but showed a single peak diurnal pattern in the active growing season (Figs. 4E and 4F).

There were also similar diurnal dynamics for ET (Figs. 4I and 4J). ET showed single-peak diurnal patterns during both seasons, with the peak values occurring at 12:00 pm. However, the peak values differed between seasons. During the non-growing season, the ET peak value was no more than 0.05 mm h^{-1}, while the ET peak values during the active growing season could be 0.28 mm h^{-1}. These results were consisting across both years measured (Figs. 4I and 4J). Additionally, the highest diurnal peak value for ET differed between measured years, with the peak value during non-growing season in 2016 higher than that of 2017 (Fig. 4I), while the peak value during active growing season in 2016 was lower than that of 2017 (Fig. 4J).

In addition, the diurnal variations of ET and environmental factors showed some fluctuations (Fig. 4), which may source from the unequal number of available data in each half-hour.
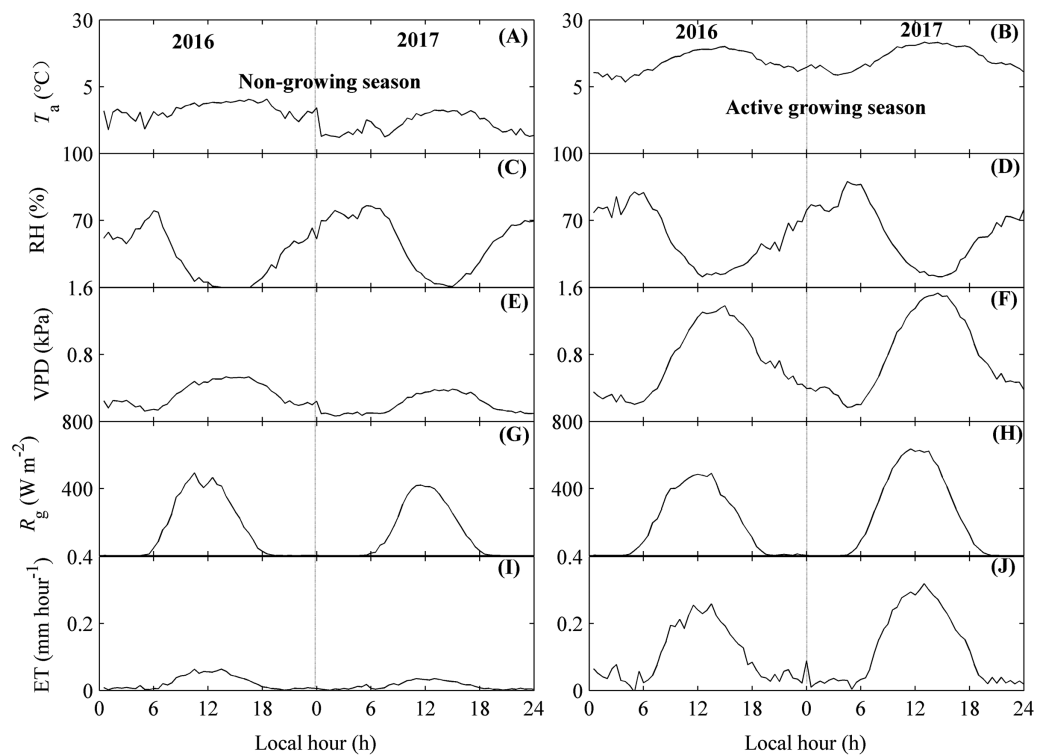
Figure 4 The diurnal dynamics of environmental factors and evapotranspiration (ET).
Environmental factors included air temperature (T_a, A and B), relative humidity (RH, C and D),
vapor pressure deficit (VPD, E and F), and global radiation (R_g, G and H). Diurnal variations of T_a, RH,
VPD, and R_g were calculated as their mean values at each 30-min period, while those of ET (I and J) were
calculated by their accumulated values during each 30-min period. The diurnal dynamics were divided
into the non-growing season (A, C, E, G, I) and the active growing season (B, D, F, H, J). Only directly
measured and passing the quality control data were used. The fluctuations in diurnal variations of ET and
environmental factors may source from the unequal number of available data in each half-hour.

Drivers of ET dynamics

Environmental factors including T_a, R_g, and VPD were found to significantly drive the
single peak diurnal patterns of ET, but their effects differed among factors and seasons
(Fig. 5). During the non-growing season, the increasing T_a, R_g, and VPD were found
to significantly affect ET, while their effects differed among factors. T_a exerted the
strongest effects on ET diurnal variations during the non-growing season. The equations
containing T_a explained 32% and 26% of the variations for ET in 2016 and 2017,
respectively (Figs. 5A and 5D). The effects of R_g and VPD on the diurnal variations of ET
during the non-growing season were similar but weaker than those of T_a. Therefore, T_a
exerted a stronger effect on the diurnal variation of ET during the non-growing season.
During the active growing season, the increasing ET was accompanied by an increase in T_a,
R_g, and VPD, while their effects differed among factors. In 2016, T_a exerted a stronger
effect on ET diurnal variations during the active growing season of 2016 (Fig. 5G),
while R_g and VPD exerted weaker effects (Figs. 5H and 5I). The equation containing T_a
explained 24% of the diurnal ET variations. In 2017, R_g had the strongest effect the diurnal
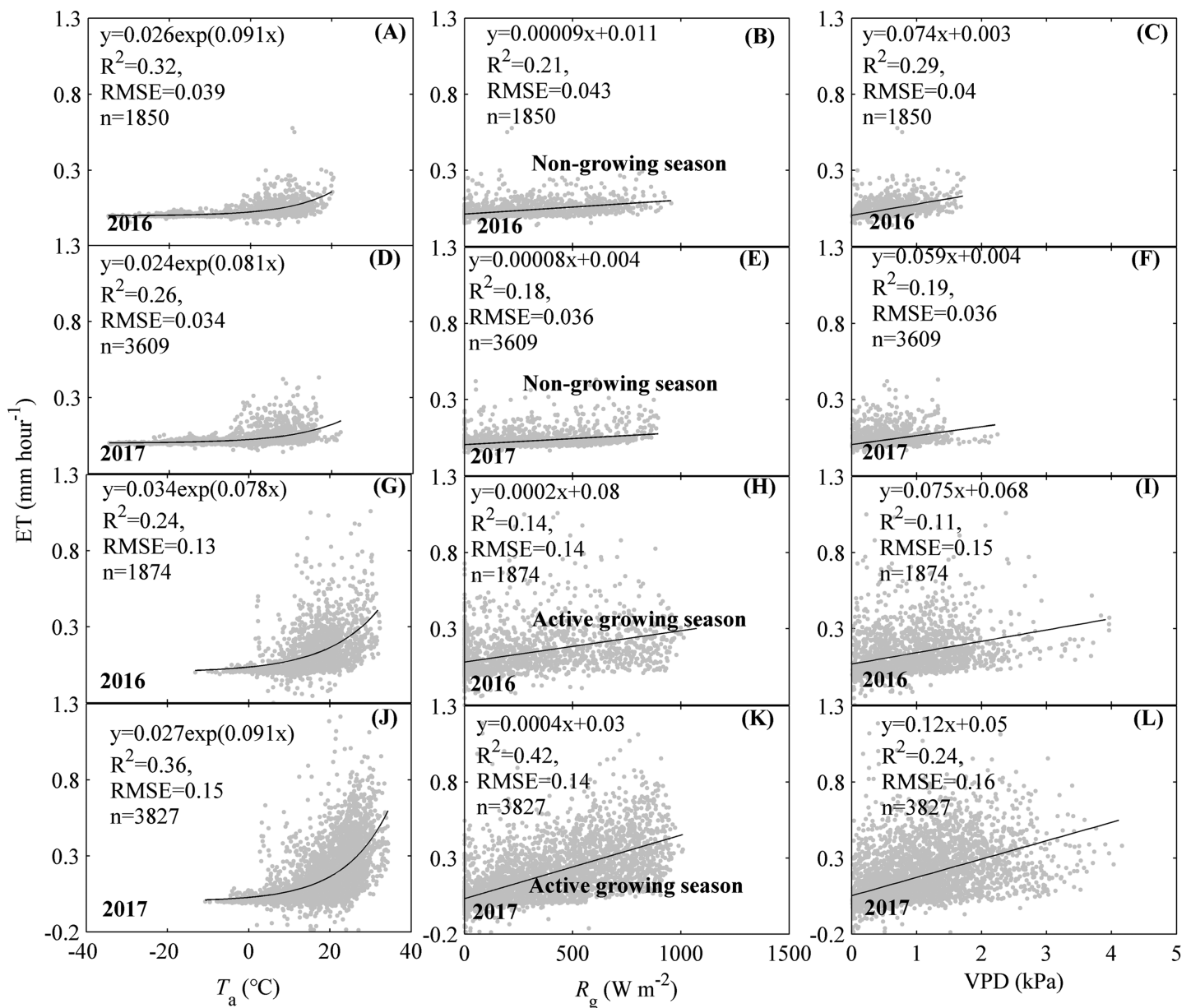
Figure 5 Effects of environmental factors on the diurnal variations of evapotranspiration (ET) at different seasons. Environmental factors included air temperature (T_a, A, D, G, J), global radiation (R_g, B, E, H, K), and vapor pressure deficit (VPD, C, F, I, L). The effects were analyzed at different seasons including the non-growing season (A–F) and the active growing season (G–L) and different years, including 2016 and 2017. Only directly measured and passing the quality control data were used.

variations of ET (Fig. 5J). The equation containing R_g explained 42% of the diurnal ET variations. T_a exerted a similar effect with R_g, which were both stronger than VPD (Figs. 5J–5L). Therefore, the diurnal ET variations during the active growing season were governed by T_a and R_g, respectively.

The seasonal variation of ET was primarily shaped by T_a and LAI, while R_g and VPD did not contribute much (Fig. 6). ET increased exponentially as T_a increased with an R^2 of 0.65 and 0.83 for 2016 and 2017, respectively (Fig. 6A). R_g only significantly increased
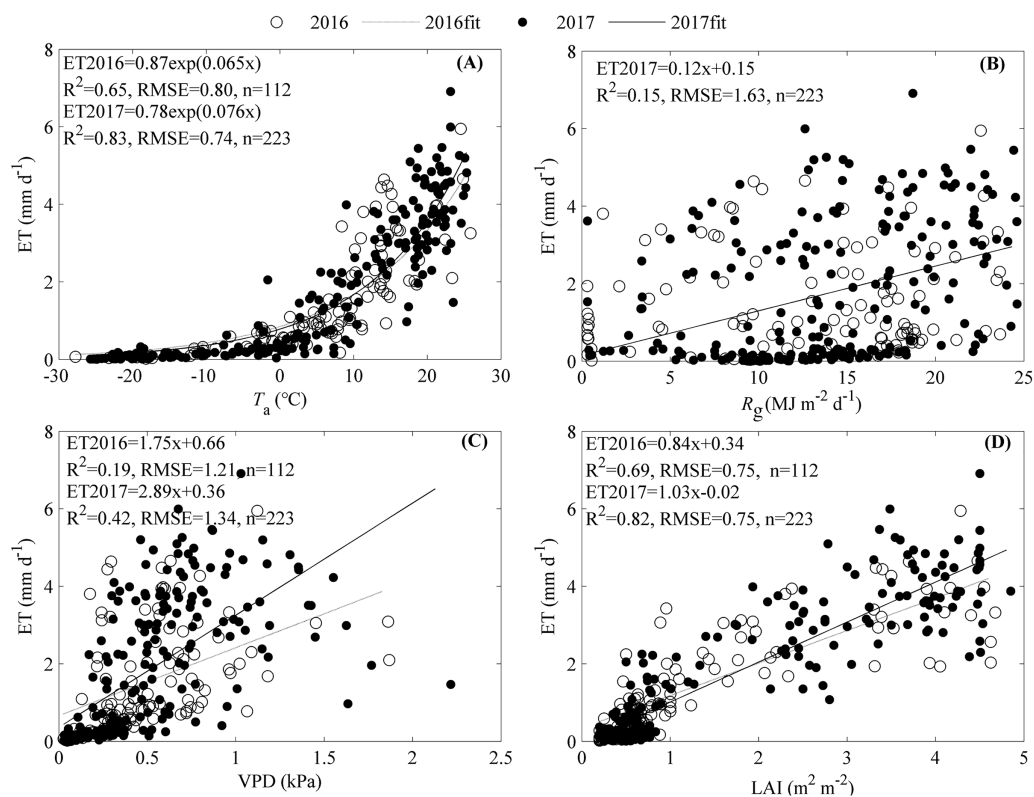
Figure 6 Effects of environmental factors on the seasonal variations of evapotranspiration (ET) during 2016 and 2017. Factors included air temperature (T_a, A), global radiation (R_g, B), vapor pressure deficit (VPD, C), and leaf area index (LAI, D). Only daily data during days having more than 20 (including 20) directly measured and passing the quality control data were used.

ET in 2017 with an R^2 of 0.15 (Fig. 6B). Though the increasing VPD significantly promoted ET, the equations containing VPD explained little of the ET seasonal variations (Fig. 6C). LAI made great contributions to the seasonal variations of ET, and as it increased, ET increased linearly with an R^2 of 0.69 for 2016 and 0.82 for 2017, respectively (Fig. 6D).

The significant correlations between ET and the environmental variables (Fig. 6) indicated that the seasonal variations of ET were shaped by multiple factors. Stepwise analysis showed that variables entering the equation describing ET seasonal variations differed between years. In 2016, only T_a and LAI entered the equation describing ET seasonal variations, with an R^2 of 0.75 and an RMSE of 0.68 mm d^{-1} (Eq. (2)). In 2017, all variables including T_a, R_g, and LAI entered the equation describing ET seasonal variations, with an R^2 of 0.86 and an RMSE of 0.66 mm d^{-1} (Eq. (3)).

$$ET = 0.038T_a + 0.604LAI + 0.467, R^2 = 0.75, RMSE = 0.68 \tag{2}$$

$$ET = 0.030T_a + 0.031R_g + 0.754LAI - 0.092, R^2 = 0.86, RMSE = 0.66 \tag{3}$$

Though many variables entered the equations describing the seasonal variations of ET (Eqs. (2) and (3)), each variable had a divergent role (Fig. 7). LAI exerted the strongest
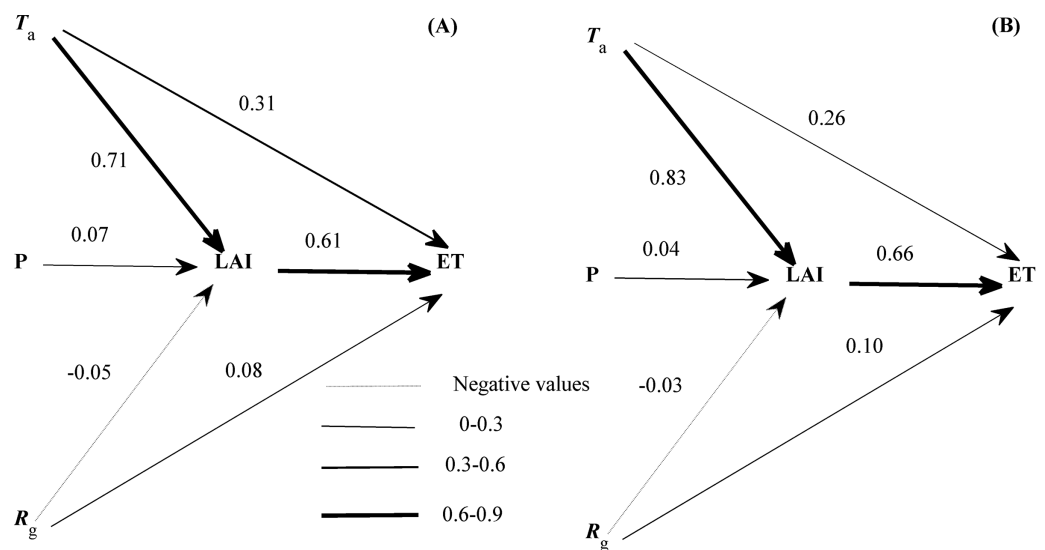
Figure 7 The path diagram between environmental factors and the seasonal variation of evapotranspiration (ET) at 2016 (A) and 2017 (B). The concerning variables included air temperature (T_a), global radiation (R_g), precipitation (P), and leaf area index (LAI). Line widths reflected the roles of each variable. Only daily data during days having more than 20 (including 20) directly measured and passing the quality control data were used.

direct effect on the seasonal variation of ET. T_a and R_g also directly affected the seasonal variation of ET but showed a weaker effect than LAI. In addition, the seasonal variation of LAI was dominated by T_a, and supported by R_g and precipitation. The roles of environmental factors in the seasonal variation of ET were comparable in both years (Fig. 7). LAI was shown to exert a direct effect on the seasonal dynamics of ET in our ecosystem.

The annual amount of ET and its related variables

The mean annual ET during the measuring period was 528.26 mm year^{-1}, which were measured as 501.91 ± 5.30 mm year^{-1} and 554.60 ± 11.24 mm year^{-1} for 2016 and 2017, respectively (Table 1). The uncertainty of annual ET sourced from gap-filling was less than 2%. The active growing season values from May to October were the primary contributors to ET and accounted for over 90% of its annual value (Table 1). July had the highest ET, exceeding 120 mm month^{-1} in both years, which was 1 month prior to the measurement of the highest precipitation (Table 1). However, June contributed the second highest ET in 2016 while August had the second highest ET in 2017.

  The annual mean air temperature (MAT) were 0.57 and 1.17 °C for 2016 and 2017, respectively, which resulted from a hot summer from May to October and a cold winter from November to April. The annual R_g were not reported as many long data gaps during the measuring period, while VPD for 2016 and 2017 were only 0.33 and 0.37 kPa, respectively. The annual precipitation were 565 and 518.50 mm for 2016 and 2017, respectively. In addition, the annual mean LAI of 2016 and 2017 were 1.53 and 1.47 m^2 m^{-2}, respectively.

Table 1 The monthly and annual values of evapotranspiration (ET), air temperature (T_a), global radiation (R_g), vapour pressure deficit (VPD), precipitation, leaf area index (LAI) during 2016 and 2017.

Year	Month	ET (mm month^{-1})	T_a (°C)	VPD (kPa)	Precipitation (mm month^{-1})	LAI (m^2 m^{-2})
2016	1	1.28 ± 0.33	−22.12	0.04	3	0.24
	2	2.67 ± 0.17	−17.48	0.08	1.8	0.30
	3	14.45 ± 0.53	−4.51	0.24	10.9	0.43
	4	25.91 ± 0.58	4.03	0.44	27.7	0.60
	5	61.64 ± 1.73	11.95	0.73	87.5	1.57
	6	101.28 ± 2.46	16.37	0.45	140.2	3.62
	7	120.93 ± 2.52	21.01	0.65	115.5	4.26
	8	95.82 ± 2.48	18.65	0.54	70.6	4.07
	9	58.48 ± 1.96	13.38	0.33	61.9	1.72
	10	10.91 ± 0.27	−0.45	0.26	27	0.66
	11	4.82 ± 0.21	−15.09	0.07	15.7	0.43
	12	3.74 ± 0.29	−18.91	0.11	3.2	0.41
	Total/mean	501.91 ± 5.30	0.57	0.33	565.00	1.53
2017	1	0.99 ± 0.12	−20.13	0.05	2.7	0.35
	2	3.14 ± 0.10	−14.60	0.10	8.6	0.33
	3	8.56 ± 0.34	−4.83	0.23	5.8	0.46
	4	33.60 ± 1.12	4.26	0.39	63.4	0.65
	5	70.58 ± 1.06	13.11	0.88	36.7	1.89
	6	98.59 ± 2.28	16.56	0.57	123.2	3.60
	7	123.85 ± 2.53	20.99	0.76	50.9	3.71
	8	112.08 ± 3.29	19.29	0.51	94.2	3.79
	9	85.54 ± 8.64	11.74	0.39	92.9	1.57
	10	11.42 ± 0.44	1.43	0.32	16.2	0.54
	11	4.93 ± 0.13	−11.42	0.10	17.4	0.51
	12	1.32 ± 0.09	−22.35	0.10	6.5	0.25
	Total/mean	554.60 ± 11.24	1.17	0.37	518.50	1.47

Note:
Values of T_a, VPD, and LAI were the mean values during the measuring period, while others were the total values.

Therefore, this forest was shown to experience a high evaporate rate, which is crucial to the global water cycle.

DISCUSSION

The quality of our measurements was key for the accurate analysis of ET dynamics and their drivers. These were evaluated using the available data portion and energy balance closure. The available data portion may be over 43.55% of the whole year as determined by the number of observations passing data quality control, which was slightly lower than that of some ChinaFLUX ecosystems (*Fu et al., 2009*; *Yu et al., 2008*; *Zhu et al., 2015a*). For example, the data coverage of three forests ranged from 43% to 54% (*Zhu et al., 2015a*), while that of three grasslands varied from 46% to 50% (*Fu et al., 2009*). Our ecosystem experienced a colder winter, which affected the eddy covariance instruments negatively, resulting in a lower data quality. The relative lower data coverage of our ecosystem was

acceptable. From the energy balance closure, we found that the energy balance regression slope of our ecosystem from OLSs was 0.54 and the EBC was around 0.62, which was lower than most ChinaFLUX ecosystems (*Li et al., 2005*) and some European forests (*Moderow et al., 2009*; *Sanchez, Caselles & Rubio, 2010*) but fell into the range of energy balance closure of FLUXNET(*Stoy et al., 2013*; *Wilson et al., 2002*). The lower EBC in our ecosystem could be attributed to three aspects. First, our ecosystem experienced a cool temperature and a multiple plant composition, which made our ecosystem have a lower EBC as the EBC would increase with the increasing mean annual air temperature (*Cui & Chui, 2019*) and the decreasing heterogeneity (*Foken, 2008*; *Stoy et al., 2013*; *Xin et al., 2018*). Second, the soil heat flux (*G*) may be underestimated, especially during the non-growing season. This was also validated by an obviously higher energy balance closure during the active growing season (Figs. 2B and 2C). *G* was the product of soil bulk density, soil heat capacity, and soil temperature variations. Our ecosystem experienced a long snow covering period, whose heat capacity was higher than the soil (*Li, Jia & Lu, 2015*). However, we calculated the *G* during snow covering period with a soil heat capacity at ice free seasons, which made soil heat capacity used in calculating *G* during snow covering period underestimated. Therefore, the *G* during the non-growing season was underestimated, which further decreased the EBC of our ecosystem. Third, we only considered the heat storage in the soil (*G*) but ignored other heat storages. Heat can be stored in the soil, biomass, air (*Moderow et al., 2009*), and biogeochemical processes (*Eshonkulov et al., 2019*), with nearly equal contributions among these components (*Lindroth, Mölder & Lagergren, 2010*). Ignoring heat storage in some components (like air and biomass) may cause the energy balance closure to be underestimated (*Eshonkulov et al., 2019*; *Franssen et al., 2010*; *Lindroth, Mölder & Lagergren, 2010*). We can conservatively state that the eddy covariance measurement in our ecosystem performed well after fully considering the data coverage and energy balance closure.

We analysed the dynamics of ET and their drivers based on EC measuring ET and environmental factors. Our results showed that the seasonal and diurnal variations of ET all exhibited a single peak pattern with the daily ET ranging from 0 to 7.75 mm d^{-1} and the hourly ET ranging from 0 to 0.28 mm h^{-1}. We also found that diurnal dynamics of ET during the non-growing season and the active growing season were driven by T_a and R_g, while seasonal ET dynamics were primarily affected by LAI. The single peak patterns of diurnal and seasonal dynamics for ET were commonly found in temperate ecosystems (*Vourlitis et al., 2002*; *Wever, Flanagan & Carlson, 2002*; *Zheng et al., 2014*; *Zhou et al., 2010*). However, our hourly and daily ET ranges differed from previous works, which may be related to a difference in climate and ecosystem types. For example, the daily ET of a Japanese temperate cypress forest ranged from 0 to 5.15 mm d^{-1} (*Kosugi et al., 2007*), while the daily ET of a Chinese warm temperate plantation ranged from 0 to 7.4 mm d^{-1} (*Tong et al., 2017*). American temperate managed forests had a daily ET ranging from 0 to 6 mm d^{-1} and hourly ET varying from 0 to 0.3 mm h^{-1} (*Sun et al., 2008*). The drivers also differed from other ecosystems (*Tong et al., 2017*; *Yoshida et al., 2010*), which may be related to the unique characteristics of our ecosystem. As a temperate mixed forest, our ecosystem experienced a unique climate with sufficient water supply but limited radiation.

Table 2 The published annual evapotranspiration (ET) in northeast Asia.

Ecosystem	Latitude (°N)	Longitude (°E)	Altitude (m.a.s.l)	Vegetation type	MAT (°C)	MAP (mm)	ET (mm year⁻¹)	Observation period	References
Changbaishan forest	42.40	128.10	736	MF	4.40	471.10	500.37	2003–2007	*Wu et al. (2015)*, *Zhang et al. (2012)*
Horqin grassland	43.29	122.28	203	GRA	6.76	342.33	633.19	2008–2013	*Li et al. (2016)*
Tongyu cropland	44.57	122.92	184	CRO	6.73	295.92	306.33	2003–2008	*Liu & Feng (2012)*
Changling grassland	44.58	123.50	171	GRA	7.50	296.05	306.80	2007–2008	*Dong et al. (2011)*
Tongyu grassland	44.59	122.52	184	GRA	6.68	298.17	303.04	2003–2008	*Liu & Feng (2012)*
Laoshan forest	45.33	127.67	340	DEF	1.79	552.00	328.53	2004	*Wang et al. (2004)*
Tomakomai forest	42.73	141.52	140	MF	6.00	1265	367	2001–2002	*Hirano et al. (2003)*
Kherlenbayan-Ulaan grassland	47.21	108.74	1235	GRA	1.2	159	144.25	2003–2006	*Li et al. (2007)*, *Liu et al. (2010)*
Yichun forest	48.10	129.23	420	MF	0.87	542	528.26	2016–2017	This study

Therefore, energy supply, which could be represented by T_a or R_g, was the primary factor shaping the dynamics of ET in our ecosystem. T_a showed a larger range than R_g (Figs. 5A–5F), which made T_a be the primary factor shaping ET diurnal dynamics when considering the diurnal variations of ET during the non-growing season. Given most data during active growing season of 2016 were missing (Fig. 3), the effects of environmental factors on ET diurnal variations were comparable to those during the non-growing season, which made T_a be the dominating factor shaping ET diurnal variation. However, R_g exhibited a larger range than T_a (Figs. 5G–5L) during the active growing season of 2017, which indicated that R_g governed the diurnal dynamics of ET. Though LAI was found to directly affect the seasonal dynamics of ET, LAI was the comprehensive representation of T_a and R_g (Fig. 7) and reflected the dominating role of energy supply in the seasonal dynamics of ET.

The unique climate resulted in an evaporation rate of 528.26 mm year⁻¹ as ET, which was almost equal to its annual precipitation. The studied ecosystem had a lower ET than those with a warmer MAT like the Horqin grassland (*Li et al., 2016*). However, our ecosystem had a higher ET than other ecosystems in this region, including those experiencing a warmer MAT like the Changbaishan forest (*Wu et al., 2015*), Tomakomai forest (*Hirano et al., 2003*), and Laoshan forest (*Wang et al., 2004*) (Table 2), or ecosystems having a higher MAT and a lower MAP (including the Tongyu cropland, Tongyu grassland, Changling grassland) (*Li et al., 2016*; *Liu & Feng, 2012*), and ecosystems experiencing a similar MAT but a lower MAP like the Kherlenbayan-Ulaan grassland (*Li et al., 2007*; *Liu et al., 2010*). Our findings indicate that the studied ecosystem evaporated more water into the atmosphere, suggesting its importance in the global water cycle.

CONCLUSIONS

In this study, we analysed the dynamics of evapotranspiration (ET) in a temperate mixed forest using an eddy covariance approach. Our results showed that 43.55% eddy

covariance measured data passed the data quality control checks with an energy balance ratio of 0.62. These results indicate the accuracy of the eddy covariance approach in our ecosystem. ET exhibited single-peak diurnal and seasonal patterns, with diurnal dynamics driven by air temperature (T_a) and global radiation (R_g) during non-growing season and active growing season, respectively, and seasonal dynamics affected by leaf area index (LAI), which all reflected the energy supply. The dynamics of ET resulted in a mean annual ET of 528.26 mm year^{-1} during 2016–2017. Therefore, the energy supply governed the dynamics of ET during all seasons and time scales in our temperate mixed forest, but variables representing the energy supply differed among seasons and time scales. The dynamics of ET show that this temperate ecosystem had an important role in global water cycles. The results of our work improve our understanding of ET dynamics in this region.

ACKNOWLEDGEMENTS

We gratefully acknowledge the reviewers for spending their valuable time to provide constructive feedback.

Funding

This research was supported by the National Key Research and Development Project of China (2018YFC1506802), the National Natural Science Foundation of China (32071585, 31500390), the open fund of the institute of atmospheric environment, China Meteorological Administration, Shenyang (2018SYIAE03, 2018SYIAE09), and the Basic Scientific Research Operating Expenses of Public Welfare Research Institutes of Shenyang Institute of Atmospheric Environment, China Meteorological Administration, Shenyang (2016SYIAEZD2). The funders had no role in study design, data collection and analysis, decision to publish, or preparation of the manuscript.

Grant Disclosures

The following grant information was disclosed by the authors:
National Key Research and Development Project of China: 2018YFC1506802.
National Natural Science Foundation of China: 32071585, 31500390.
Institute of Atmospheric Environment, China Meteorological Administration, Shenyang: 2018SYIAE03, 2018SYIAE09.
Basic Scientific Research Operating Expenses of Public Welfare Research Institutes of Shenyang Institute of Atmospheric Environment, China Meteorological Administration, Shenyang: 2016SYIAEZD2.

Competing Interests

The authors declare that they have no competing interests.

Author Contributions

- Xiaoying Wang conceived and designed the experiments, prepared figures and/or tables, and approved the final draft.
- Xianjin Zhu conceived and designed the experiments, performed the experiments, prepared figures and/or tables, authored or reviewed drafts of the article, and approved the final draft.
- Mingjie Xu performed the experiments, prepared figures and/or tables, and approved the final draft.
- RiHong Wen conceived and designed the experiments, performed the experiments, authored or reviewed drafts of the article, and approved the final draft.
- Qingyu Jia analyzed the data, authored or reviewed drafts of the article, and approved the final draft.
- YanBing Xie analyzed the data, authored or reviewed drafts of the article, and approved the final draft.
- Hongda Ma analyzed the data, authored or reviewed drafts of the article, and approved the final draft.

Data Availability

The raw data is available in the Supplemental File.

Supplemental Information

Supplemental information for this article can be found online at http://dx.doi.org/10.7717/peerj.13549#supplemental-information.

REFERENCES

Anapalli SS, Fisher DK, Pinnamaneni SR, Reddy KN. 2020. Quantifying evapotranspiration and crop coefficients for cotton (Gossypium hirsutum L.) using an eddy covariance approach. *Agricultural Water Management* **233(55)**:106091 DOI 10.1016/j.agwat.2020.106091.

Aubinet M, Grelle A, Ibrom A, Rannik U, Moncrieff J, Foken T, Kowalski AS, Martin PH, Berbigier P, Bernhofer C, Clement R, Elbers J, Granier A, Grunwald T, Morgenstern K, Pilegaard K, Rebmann C, Snijders W, Valentini R, Vesala T. 2000. Estimates of the annual net carbon and water exchange of forests: the EUROFLUX methodology. *Advances in Ecological Research* **30(D4)**:113–175 DOI 10.1016/S0065-2504(08)60018-5.

Baldocchi DD, Ryu Y. 2011. A synthesis of forest evaporation fluxes–from days to years–as measured with eddy covariance. In: Levia DF, Carlyle-Moses D, Tanaka T, eds. *Forest Hydrology and Biogeochemistry*. Dordrecht: Springer Netherlands, 101–116.

Chapin FS, Matson PA, Mooney HA. 2012. *Principles of terrestrial ecosystem ecology*. New York: Springer.

Cristiano PM, Campanello PI, Bucci SJ, Rodriguez SA, Lezcano OA, Scholz FG, Madanes N, Di Francescantonio D, Carrasco LO, Zhang Y-J, Goldstein G. 2015. Evapotranspiration of subtropical forests and tree plantations: a comparative analysis at different temporal and spatial scales. *Agricultural and Forest Meteorology* **203(3)**:96–106 DOI 10.1016/j.agrformet.2015.01.007.

Cui W, Chui TFM. 2019. Temporal and spatial variations of energy balance closure across FLUXNET research sites. *Agricultural and Forest Meteorology* **271(12)**:12–21 DOI 10.1016/j.agrformet.2019.02.026.

Desai AR, Bolstad PV, Cook BD, Davis KJ, Carey EV. 2005. Comparing net ecosystem exchange of carbon dioxide between an old-growth and mature forest in the upper Midwest, USA. *Agricultural and Forest Meteorology* **128(1–2)**:33–55 DOI 10.1016/j.agrformet.2004.09.005.

Dong G, Guo J, Chen J, Sun G, Gao S, Hu L, Wang Y. 2011. Effects of spring drought on carbon sequestration, evapotranspiration and water use efficiency in the songnen meadow steppe in northeast China. *Ecohydrology* **4**:211–224 DOI 10.1002/eco.200.

Drexler JZ, Snyder RL, Spano D, Paw KTU. 2004. A review of models and micrometeorological methods used to estimate wetland evapotranspiration. *Hydrological Processes* **18**:2071–2101 DOI 10.1002/(ISSN)1099-1085.

Eshonkulov R, Poyda A, Ingwersen J, Pulatov A, Streck T. 2019. Improving the energy balance closure over a winter wheat field by accounting for minor storage terms. *Agricultural and Forest Meteorology* **264**:283–296 DOI 10.1016/j.agrformet.2018.10.012.

Falge E, Baldocchi D, Olson R, Anthoni P, Aubinet M, Bernhofer C, Burba G, Ceulemans G, Clement R, Dolman H, Granier A, Gross P, Grunwald T, Hollinger D, Jensen NO, Katul G, Keronen P, Kowalski A, Lai CT, Law BE, Meyers T, Moncrieff J, Moors E, Munger JW, Pilegaard K, Rannik U, Rebmann C, Suyker A, Tenhunen J, Tu K, Verma S, Vesala T, Wilson K, Wofsy S. 2001a. Gap filling strategies for long term energy flux data sets. *Agricultural and Forest Meteorology* **107(1)**:71–77 DOI 10.1016/S0168-1923(00)00235-5.

Falge E, Baldocchi D, Olson R, Anthoni P, Aubinet M, Bernhofer C, Burba G, Ceulemans R, Clement R, Dolman H, Granier A, Gross P, Grunwald T, Hollinger D, Jensen NO, Katul G, Keronen P, Kowalski A, Lai CT, Law BE, Meyers T, Moncrieff H, Moors E, Munger JW, Pilegaard K, Rannik U, Rebmann C, Suyker A, Tenhunen J, Tu K, Verma S, Vesala T, Wilson K, Wofsy S. 2001b. Gap filling strategies for defensible annual sums of net ecosystem exchange. *Agricultural and Forest Meteorology* **107(1)**:43–69 DOI 10.1016/S0168-1923(00)00225-2.

Foken T. 2008. The energy balance closure problem: an overview. *Ecological Applications* **18(6)**:1351–1367 DOI 10.1890/06-0922.1.

Franssen HJH, Stöckli R, Lehner I, Rotenberg E, Seneviratne SI. 2010. Energy balance closure of eddy-covariance data: a multisite analysis for European FLUXNET stations. *Agricultural and Forest Meteorology* **150(12)**:1553–1567 DOI 10.1016/j.agrformet.2010.08.005.

Fu Y, Zheng Z, Yu G, Hu Z, Sun X, Shi P, Wang Y, Zhao X. 2009. Environmental influences on carbon dioxide fluxes over three grassland ecosystems in China. *Biogeosciences* **6(12)**:2879–2893 DOI 10.5194/bg-6-2879-2009.

Gielen B, Verbeeck H, Neirynck J, Sampson DA, Vermeiren F, Janssens IA. 2010. Decadal water balance of a temperate Scots pine forest (Pinus sylvestris L.) based on measurements and modelling. *Biogeosciences* **7(4)**:1247–1261 DOI 10.5194/bg-7-1247-2010.

Hirano T, Hirata R, Fujinuma Y, Saigusa N, Yamamoto S, Harazono Y, Takada M, Inukai K, Inoue G. 2003. CO2 and water vapor exchange of a larch forest in Northern Japan. *Tellus B: Chemical and Physical Meteorology* **55(2)**:244–257 DOI 10.3402/tellusb.v55i2.16753.

Hollinger DY, Kelliher FM, Byers JN, Hunt JE, McSeveny TM, Weir PL. 1994. Carbon dioxide exchange between an undisturbed old-growth temperate forest and the atmosphere. *Ecology* **75(1)**:134–150 DOI 10.2307/1939390.

Horst TW, Lenschow DH. 2009. Attenuation of scalar fluxes measured with spatially-displaced sensors. *Boundary-Layer Meteorology* **130(2)**:275–300 DOI 10.1007/s10546-008-9348-0.

Kljun N, Calanca P, Rotach MW, Schmid HP. 2004. A simple parameterisation for flux footprint predictions. *Boundary-Layer Meteorology* **112(3)**:503–523 DOI 10.1023/B:BOUN.0000030653.71031.96.

Kool D, Agam N, Lazarovitch N, Heitman JL, Sauer TJ, Ben-Gal A. 2014. A review of approaches for evapotranspiration partitioning. *Agricultural and Forest Meteorology* **184**:56–70 DOI 10.1016/j.agrformet.2013.09.003.

Kosugi Y, Takanashi S, Tanaka H, Ohkubo S, Tani M, Yano M, Katayama T. 2007. Evapotranspiration over a Japanese cypress forest. I. Eddy covariance fluxes and surface conductance characteristics for 3 years. *Journal of Hydrology* **337(3–4)**:269–283 DOI 10.1016/j.jhydrol.2007.01.039.

Kumagai T, Saitoh TM, Sato Y, Takahashi H, Manfroi OJ, Morooka T, Kuraji K, Suzuki M, Yasunari T, Komatsu H. 2005. Annual water balance and seasonality of evapotranspiration in a Bornean tropical rainforest. *Agricultural and Forest Meteorology* **128(1–2)**:81–92 DOI 10.1016/j.agrformet.2004.08.006.

Kume T, Tanaka N, Kuraji K, Komatsu H, Yoshifuji N, Saitoh TM, Suzuki M, Kumagai T. 2011. Ten-year evapotranspiration estimates in a Bornean tropical rainforest. *Agricultural and Forest Meteorology* **151(9)**:1183–1192 DOI 10.1016/j.agrformet.2011.04.005.

Li SG, Asanuma J, Kotani A, Davaa G, Oyunbaatar D. 2007. Evapotranspiration from a Mongolian steppe under grazing and its environmental constraints. *Journal of Hydrology* **333(1)**:133–143 DOI 10.1016/j.jhydrol.2006.07.021.

Li NN, Jia L, Lu J. 2015. An improved algorithm to estimate the surface soil heat flux over a heterogeneous surface: a case study in the Heihe River Basin. *Science China-Earth Sciences* **58(7)**:1169–1181 DOI 10.1007/s11430-014-5041-y.

Li ZL, Tang RL, Wan ZM, Bi YY, Zhou CH, Tang BH, Yan GJ, Zhang XY. 2009. A review of current methodologies for regional evapotranspiration estimation from remotely sensed data. *Sensors* **9(5)**:3801–3853 DOI 10.3390/s90503801.

Li HD, Wang AZ, Yuan FH, Guan DX, Jin CJ, Wu JB, Zhao TB. 2016. Evapotranspiration dynamics over a temperate meadow ecosystem in Eastern Inner Mongolia, China. *Environmental Earth Sciences* **75(11)**:749 DOI 10.1007/s12665-016-5786-z.

Li Z, Yu G, Wen X, Zhang L, Ren C, Fu Y. 2005. Energy balance closure at ChinaFLUX sites. *Science in China Series D: Earth Sciences* **48**:51–62 DOI 10.1360/05zd0005.

Li ZH, Zhang YP, Wang SS, Yuan GF, Yang Y, Cao M. 2010. Evapotranspiration of a tropical rain forest in Xishuangbanna, Southwest China. *Hydrological Processes* **24(D20)**:2405–2416 DOI 10.1002/hyp.7643.

Lindroth A, Mölder M, Lagergren F. 2010. Heat storage in forest biomass improves energy balance closure. *Biogeosciences* **7(1)**:301–313 DOI 10.5194/bg-7-301-2010.

Liu HZ, Feng JW. 2012. Seasonal and interannual variations of evapotranspiration and energy exchange over different land surfaces in a semiarid area of China. *Journal of Applied Meteorology and Climatology* **51(10)**:1875–1888 DOI 10.1175/JAMC-D-11-0229.1.

Liu S, Li SG, Yu GR, Asanuma J, Sugita M, Zhang LM, Hu ZM, Wei YF. 2010. Seasonal and interannual variations in water vapor exchange and surface water balance over a grazed steppe in central Mongolia. *Agricultural Water Management* **97(6)**:857–864 DOI 10.1016/j.agwat.2010.01.016.

Ma N, Zhang Y, Guo Y, Gao H, Zhang H, Wang Y. 2015. Environmental and biophysical controls on the evapotranspiration over the highest alpine steppe. *Journal of Hydrology* **529(4)**:980–992 DOI 10.1016/j.jhydrol.2015.09.013.

Moderow U, Aubinet M, Feigenwinter C, Kolle O, Lindroth A, Molder M, Montagnani L, Rebmann C, Bernhofer C. 2009. Available energy and energy balance closure at four coniferous forest sites across Europe. *Theoretical and Applied Climatology* **98(3–4)**:397–412 DOI 10.1007/s00704-009-0175-0.

Moncrieff J, Clement R, Finnigan J, Meyers T. 2005. Averaging, detrending, and filtering of eddy covariance time series. In: Lee X, Massman W, Law B, eds. *Handbook of Micrometeorology: A Guide for Surface Flux Measurement and Analysis*. Dordrecht: Springer Netherlands, 7–31.

Moncrieff JB, Massheder JM, deBruin H, Elbers J, Friborg T, Heusinkveld B, Kabat P, Scott S, Soegaard H, Verhoef A. 1997. A system to measure surface fluxes of momentum, sensible heat, water vapour and carbon dioxide. *Journal of Hydrology* **189(Suppl. II)**:589–611 DOI 10.1016/S0022-1694(96)03194-0.

Ohtsuka T, Akiyama T, Hashimoto Y, Inatomi M, Sakai T, Jia S, Mo W, Tsuda S, Koizumi H. 2005. Biometric based estimates of net primary production (NPP) in a cool-temperate deciduous forest stand beneath a flux tower. *Agricultural and Forest Meteorology* **134(1–4)**:27–38 DOI 10.1016/j.agrformet.2005.11.005.

Okada K, Takagi K, Nishida Y. 2019. Effects of forestry management and environmental factors on water and light use efficiencies in a cool-temperate mixed forest in Northern Japan. *Journal of Agricultural Meteorology* **75(4)**:183–192 DOI 10.2480/agrmet.D-19-00006.

Pita G, Gielen B, Zona D, Rodrigues A, Rambal S, Janssens IA, Ceulemans R. 2013. Carbon and water vapor fluxes over four forests in two contrasting climatic zones. *Agricultural and Forest Meteorology* **180**:211–224 DOI 10.1016/j.agrformet.2013.06.003.

Rana G, Katerji N. 2000. Measurement and estimation of actual evapotranspiration in the field under Mediterranean climate: a review. *European Journal of Agronomy* **13(2–3)**:125–153 DOI 10.1016/S1161-0301(00)00070-8.

Reichstein M, Falge E, Baldocchi D, Papale D, Aubinet M, Berbigier P, Bernhofer C, Buchmann N, Gilmanov T, Granier A, Grunwald T, Havrankova K, Ilvesniemi H, Janous D, Knohl A, Laurila T, Lohila A, Loustau D, Matteucci G, Meyers T, Miglietta F, Ourcival JM, Pumpanen J, Rambal S, Rotenberg E, Sanz M, Tenhunen J, Seufert G, Vaccari F, Vesala T, Yakir D, Valentini R. 2005. On the separation of net ecosystem exchange into assimilation and ecosystem respiration: review and improved algorithm. *Global Change Biology* **11(9)**:1424–1439 DOI 10.1111/j.1365-2486.2005.001002.x.

Saigusa N, Yamamoto S, Murayama S, Kondo H, Nishimura N. 2002. Gross primary production and net ecosystem exchange of a cool-temperate deciduous forest estimated by the eddy covariance method. *Agricultural and Forest Meteorology* **112(3–4)**:203–215 DOI 10.1016/S0168-1923(02)00082-5.

Sanchez JM, Caselles V, Rubio EM. 2010. Analysis of the energy balance closure over a FLUXNET boreal forest in Finland. *Hydrology and Earth System Sciences* **14(8)**:1487–1497 DOI 10.5194/hess-14-1487-2010.

Schaefer KVR, Tripathee R, Artigas F, Morin TH, Bohrer G. 2014. Carbon dioxide fluxes of an urban tidal marsh in the Hudson-Raritan estuary. *Journal of Geophysical Research: Biogeosciences* **119(11)**:2065–2081 DOI 10.1002/2014JG002703.

Song Q-H, Braeckevelt E, Zhang Y-P, Sha L-Q, Zhou W-J, Liu Y-T, Wu C-S, Lu Z-Y, Klemm O. 2017. Evapotranspiration from a primary subtropical evergreen forest in Southwest China. *Ecohydrology* **10(4)**:e1826 DOI 10.1002/eco.1826.

Soubie R, Heinesch B, Granier A, Aubinet M, Vincke C. 2016. Evapotranspiration assessment of a mixed temperate forest by four methods: eddy covariance, soil water budget, analytical and

model. *Agricultural and Forest Meteorology* **228(3)**:191–204
DOI 10.1016/j.agrformet.2016.07.001.

Stoy PC, Mauder M, Foken T, Marcolla B, Boegh E, Ibrom A, Arain MA, Arneth A, Aurela M, Bernhofer C, Cescatti A, Dellwik E, Duce P, Gianelle D, van Gorsel E, Kiely G, Knohl A, Margolis H, McCaughey H, Merbold L, Montagnani L, Papale D, Reichstein M, Saunders M, Serrano-Ortiz P, Sottocornola M, Spano D, Vaccari F, Varlagin A. 2013. A data-driven analysis of energy balance closure across FLUXNET research sites: the role of landscape scale heterogeneity. *Agricultural and Forest Meteorology* **171–172(5)**:137–152
DOI 10.1016/j.agrformet.2012.11.004.

Sun G, Noormets A, Chen J, McNulty SG. 2008. Evapotranspiration estimates from eddy covariance towers and hydrologic modeling in managed forests in Northern Wisconsin, USA. *Agricultural and Forest Meteorology* **148(2)**:257–267 DOI 10.1016/j.agrformet.2007.08.010.

Tanaka N, Kume T, Yoshifuji N, Tanaka K, Takizawa H, Shiraki K, Tantasirin C, Tangtham N, Suzuki M. 2008. A review of evapotranspiration estimates from tropical forests in Thailand and adjacent regions. *Agricultural and Forest Meteorology* **148**:807–819
DOI 10.1016/j.agrformet.2008.01.011.

Tong XJ, Zhang JS, Meng P, Li J, Zheng N. 2017. Environmental controls of evapotranspiration in a mixed plantation in North China. *International Journal of Biometeorology* **61**:227–238
DOI 10.1007/s00484-016-1205-0.

Tsuruta K, Kosugi Y, Takanashi S, Tani M. 2016. Inter-annual variations and factors controlling evapotranspiration in a temperate Japanese cypress forest. *Hydrological Processes* **30**:5012–5026
DOI 10.1002/hyp.10977.

Vickers D, Mahrt L. 1997. Quality control and flux sampling problems for tower and aircraft data. *Journal of Atmospheric and Oceanic Technology* **14**:512–526
DOI 10.1175/1520-0426(1997)014<0512:QCAFSP>2.0.CO;2.

Vourlitis GL, Priante N, Hayashi MMS, Nogueira JD, Caseiro FT, Campelo JH. 2002. Seasonal variations in the evapotranspiration of a transitional tropical forest of Mato Grosso, Brazil. *Water Resources Research* **38**:30-1–30-11 DOI 10.1029/2000wr000122.

Wang K, Dickinson RE. 2012. A review of global terrestrial evapotranspiration: observation, modeling, climatology, and climatic variability. *Reviews of Geophysics* **50(2)**:RG2005
DOI 10.1029/2011RG000373.

Wang G, Huang J, Guo W, Zuo J, Wang J, Bi J, Huang Z, Shi J. 2010. Observation analysis of land-atmosphere interactions over the Loess Plateau of Northwest China. *Journal of Geophysical Research* **115(D24)**:D00K17 DOI 10.1029/2009JD013372.

Wang S, Pan M, Mu Q, Shi X, Mao J, Bruemmer C, Jassal RS, Krishnan P, Li J, Black TA. 2015. Comparing evapotranspiration from eddy covariance measurements, water budgets, remote sensing, and land surface models over Canada. *Journal of Hydrometeorology* **16(4)**:1540–1560
DOI 10.1175/JHM-D-14-0189.1.

Wang HM, Saigusa N, Yamamoto S, Kondo H, Hirano T, Toriyama A, Fujinuma Y. 2004. Net ecosystem CO2 exchange over a larch forest in Hokkaido, Japan. *Atmospheric Environment* **38(40)**:7021–7032 DOI 10.1016/j.atmosenv.2004.02.071.

Webb EK, Pearman GL, Leuning R. 1980. Correction of flux measurement for density effects due to heat and water vapor transfer. *Quarterly Journal of the Royal Meteorological Society* **106**:85–100 DOI 10.1002/(ISSN)1477-870X.

Wehr R, Commane R, Munger JW, McManus JB, Nelson DD, Zahniser MS, Saleska SR, Wofsy SC. 2017. Dynamics of canopy stomatal conductance, transpiration, and evaporation in a

temperate deciduous forest, validated by carbonyl sulfide uptake. *Biogeosciences* **14(2)**:389–401 DOI 10.5194/bg-14-389-2017.

Wen XF, Wang HM, Wang JL, Yu GR, Sun XM. 2010. Ecosystem carbon exchanges of a subtropical evergreen coniferous plantation subjected to seasonal drought, 2003–2007. *Biogeosciences* **7(1)**:357–369 DOI 10.5194/bg-7-357-2010.

Wever LA, Flanagan LB, Carlson PJ. 2002. Seasonal and interannual variation in evapotranspiration, energy balance and surface conductance in a Northern temperate grassland. *Agricultural and Forest Meteorology* **112(1)**:31–49 DOI 10.1016/S0168-1923(02)00041-2.

Wilson K, Goldstein A, Falge E, Aubinet M, Baldocchi D, Berbigier P, Bernhofer C, Ceulemans R, Dolman H, Field C, Grelle A, Ibrom A, Law BE, Kowalski A, Meyers T, Moncrieff J, Monson R, Oechel W, Tenhunen J, Valentini R, Verma S. 2002. Energy balance closure at FLUXNET sites. *Agricultural and Forest Meteorology* **113(1–4)**:223–243 DOI 10.1016/S0168-1923(02)00109-0.

Wu J, Jing Y, Guan D, Yang H, Niu L, Wang A, Yuan F, Jin C. 2013. Controls of evapotranspiration during the short dry season in a temperate mixed forest in Northeast China. *Ecohydrology* **6(3)**:775–782 DOI 10.1002/eco.1299.

Wu JB, Zhou XY, Wang AZ, Yuan FH. 2015. Comparative measurements of water vapor fluxes over a tall forest using open- and closed-path eddy covariance system. *Atmospheric Measurement Techniques* **8(10)**:4123–4131 DOI 10.5194/amt-8-4123-2015.

Xin Y-F, Chen F, Zhao P, Barlage M, Blanken P, Chen Y-L, Chen B, Wang Y-J. 2018. Surface energy balance closure at ten sites over the Tibetan plateau. *Agricultural and Forest Meteorology* **259(1–4)**:317–328 DOI 10.1016/j.agrformet.2018.05.007.

Xu MJ, Wen XF, Wang HM, Zhang WJ, Dai XQ, Song J, Wang YD, Fu XL, Liu YF, Sun XM, Yu GR. 2014. Effects of climatic factors and ecosystem responses on the inter-annual variability of evapotranspiration in a coniferous plantation in subtropical China. *PLOS ONE* **9(1)**:e85593 DOI 10.1371/journal.pone.0085593.

Yoshida M, Ohta T, Kotani A, Maximov T. 2010. Environmental factors controlling forest evapotranspiration and surface conductance on a multi-temporal scale in growing seasons of a Siberian larch forest. *Journal of Hydrology* **395(3–4)**:180–189 DOI 10.1016/j.jhydrol.2010.10.023.

Yu GR, Zhang LM, Sun XM, Fu YL, Wen XF, Wang QF, Li SG, Ren CY, Song X, Liu YF, Han SJ, Yan JH. 2008. Environmental controls over carbon exchange of three forest ecosystems in Eastern China. *Global Change Biology* **14(11)**:2555–2571 DOI 10.1111/j.1365-2486.2008.01663.x.

Yue P, Zhang Q, Zhang L, Li H, Yang Y, Zeng J, Wang S. 2019. Long-term variations in energy partitioning and evapotranspiration in a semiarid grassland in the Loess Plateau of China. *Agricultural and Forest Meteorology* **278(D24)**:107671 DOI 10.1016/j.agrformet.2019.107671.

Zhang JH, Han SJ, Yu GR. 2006. Seasonal variation in carbon dioxide exchange over a 200-year-old Chinese broad-leaved Korean pine mixed forest. *Agricultural and Forest Meteorology* **137(3–4)**:150–165 DOI 10.1016/j.agrformet.2006.02.004.

Zhang XJ, Jin CJ, Guan DX, Wang AZ, Wu JB, Yuan FH. 2012. Long-term eddy covariance monitoring of evapotranspiration and its environmental factors in a temperate mixed forest in Northeast China. *Journal of Hydrologic Engineering* **17(9)**:965–974 DOI 10.1061/(asce)he.1943-5584.0000549.

Zhang JH, Yu GR, Han SJ, Guan DX, Sun XM. 2006b. Seasonal and annual variation of CO2 flux above a broadleaved Korean pine mixed forest. *Science in China Series D: Earth Sciences* **49(S2)**:63–73 DOI 10.1007/s11430-006-8063-2.

Zheng H, Wang Q, Zhu X, Li Y, Yu G. 2014. Hysteresis responses of evapotranspiration to meteorological factors at a diel timescale: patterns and causes. *PLOS ONE* **9(6)**:e98857 DOI 10.1371/journal.pone.0098857.

Zhou L, Zhou GS, Liu SH, Sui XH. 2010. Seasonal contribution and interannual variation of evapotranspiration over a reed marsh (Phragmites australis) in Northeast China from 3-year eddy covariance data. *Hydrological Processes* **24(8)**:1039–1047 DOI 10.1002/hyp.7545.

Zhu X-J, Yu G-R, Hu Z-M, Wang Q-F, He H-L, Yan J-H, Wang H-M, Zhang J-H. 2015a. Spatiotemporal variations of T/ET (the ratio of transpiration to evapotranspiration) in three forests of Eastern China. *Ecological Indicators* **52**:411–421 DOI 10.1016/j.ecolind.2014.12.030.

Zhu X-J, Yu G-R, Wang Q-F, Hu Z-M, Zheng H, Li S-G, Sun X-M, Zhang Y-P, Yan J-H, Wang H-M, Zhao F-H, Zhang J-H, Shi P-L, Li Y-N, Zhao L, Zhang F-W, Hao Y-B. 2015b. Spatial variability of water use efficiency in China's terrestrial ecosystems. *Global and Planetary Change* **129(11)**:37–44 DOI 10.1016/j.gloplacha.2015.03.003.